JOURNAL OF NEUROTRAUMA 25:38–51 (January 2008)

DOI: 10.1089/neu.2007.0348

Mechanical Properties of Dura Mater from the Rat Brain and Spinal Cord

JASON T. MAIKOS, RAGI A.I. ELIAS, and DAVID I. SHREIBER

ABSTRACT

The dura mater is the outermost and most substantial meningial layer of central nervous system (CNS) tissue that acts as a protective membrane for the brain and spinal cord. In animal models of traumatic brain injury and spinal cord injury, mechanical insults are often delivered directly to the dura to injure the underlying tissue. As such, including a description of the mechanical properties of dura mater is critical for biomechanical analyses of these models. We have characterized the mechanical response of dura mater from the rat brain and spinal cord in uniaxial tension. Testing was performed at low (0.0014 sec^{-1}) and high (19.42 sec^{-1}) strain rates. Both rat cranial dura and spinal dura demonstrated non-linear stress-strain responses characteristic of collagenous soft tissues. The non-linear increase in stress lagged in the spinal dura compared to the cranial dura. The slow rate data was fit to a one-term Ogden hyperelastic constitutive law, and significant differences were observed for the stiffness, G, and the parameter, α, which nominally introduces non-linearity. High strain rate stress-relaxation tests were performed to 10% strain, which was held for 10 sec. The relaxation was fit to a four-term Prony series exponential decay. Cranial dura and spinal dura demonstrated similar overall relaxation, but significant differences were identified in the distribution of the relaxation over the Prony series parameters, which demonstrated that cranial dura tended to relax faster. Polarized light microscopy revealed that the structural entities of spinal dura were aligned in the axial direction, whereas cranial dura did not demonstrate a preferential alignment. This was confirmed qualitatively with Masson's Tri-chrome and Verhoeff's Van Gieson staining for collagen and elastin, which also indicated greater elastin content for the spinal dura than for the cranial dura.

Key words: constitutive modeling; injury biomechanics; spinal cord injury; tissue mechanics; traumatic brain injury; viscoelasticity

INTRODUCTION

THE DURA MATER is the outermost and most substantial meningial layer of central nervous system (CNS) tissue that acts as a protective membrane for the brain and spinal cord (Weed, 1938). *In vivo,* dura mater is subjected to stresses from stretching during movement and from cerebrospinal fluid (CSF) pressure changes (Patin et al., 1993). The dura is composed primarily of collagen fibers interspersed with fibroblasts and elastin, and is generally flexible and elastic when stretched and deformed (Vandenabeele et al., 1996). The microstructural characteristics of dura mater fibers can vary with anatomy. For instance, human lumbar dura fibers tend to be structurally aligned in the longitudinal direction, thereby providing mechanical anisotropic properties, whereas human cra-

Department of Biomedical Engineering, Rutgers, The State University of New Jersey, Piscataway, New Jersey.

nial dura fibers tend to lack directional orientation and lead to isotropic mechanical properties (McGarvey et al., 1984; Patin et al., 1993; Runza et al., 1999). Uniaxial tension experiments on human spinal dura mater (~100 MPa) (Patin et al., 1993; Runza et al., 1999) and bovine spinal dura mater (~60 MPa) (Runza et al., 1999) demonstrate that these tissues are considerably stiffer than the spinal cords they surround (elastic modulus of ~1 MPa for human and bovine spinal cord in tension and compression) (Bilston and Thibault, 1996; Ichihara et al., 2001). Similarly, human cranial dura mater (elastic modulus in tension, ~60 MPa) (McGarvey et al., 1984) is much stiffer than human brain tissue (<1 KPa) (Prange and Margulies, 2002). These large differences underlay the functions of the dura, especially in protection of central nervous system tissue, as well as allowing for pressure variations and movement (van Noort et al., 1981).

Both spinal cord injury (SCI) and traumatic brain injury (TBI) are prevalent and costly problems in the United States (Kraus and McArthur, 1996; Berkowitz, 1998), and understanding the physical and functional responses of the spinal cord and brain structures to trauma is necessary to design rational means and methods of injury prevention, as well as to develop effective treatments. Animal models continue to be the gold standard for identifying the physiological and functional consequences of TBI and SCI, and by far, rat and mouse models are most often employed (Stokes and Jakeman, 2002; Young, 2002; Guertin, 2005). Many of these models—such as fluid percussion, weight drop, and electromagnetic or pneumatic impactors (Dixon et al., 1987; Stokes et al., 1992; Meaney et al., 1994; Ueno et al., 1995; Young, 2002)—deliver the mechanical insult across the intact dura mater. Thus, to evaluate the tissue biomechanics associated with these models, particularly with computational simulations, the contribution of the dura mater to the overall mechanical response must be included. Interestingly, although rats are by far the most commonly used experimental animal to study TBI and SCI, only a few investigations have been presented for the material properties of rat central nervous system tissue of any kind (Gefen et al., 2003; Fiford and Bilston, 2005). While there have been investigations into the human, bovine, and canine dura, to our knowledge, there are no published reports of rat dura properties, and identifying these properties is an important component in accurately modeling injury biomechanics in these and similar commonly employed models.

The present study was aimed primarily at identifying the mechanical properties of rat dura mater from the brain and spinal cord at low and high strain rates. Dura from both regions was found to follow hyperelastic and viscoelastic behavior. Cranial dura demonstrated more acute non-linear stiffening. Polarized light microscopy and histology suggest that the differences in constitutive behavior are linked to the structural organization and composition of the tissues.

METHODS

Sample Preparation

Adult Long-Evans hooded rats (77 ± 5 days old; Simonsen Labs, Gilroy, CA) were euthanized with a lethal dose of sodium pentabarbitol (65 mg/kg), and the spinal columns were immediately removed. The laminae were removed from the first cervical vertebra (C1) to the first lumbar vertebrae (L1). The dura was then marked into three 30-mm segments with a permanent marker to designate original *in situ* length. Within each 30-mm section, the central 12 mm was also marked (Fig. 1A). The dura was carefully removed from the dorsal surface of the spinal cord and placed in fresh phosphate-buffered saline (PBS; 200 mg/L potassium chloride, 200 mg/L potassium phosphate monobasic, 8000 mg/L sodium chloride, 1150 mg/L sodium phosphate dibasic; M.P. Biomedicals, Solon, OH). Dura samples were cut into strips of 30 mm based on the *in situ* markings and kept hydrated in fresh PBS. Typically, three samples were harvested per cord, unless damage was noted upon visual inspection. Length and width measurements were taken at the central 12 mm with digital calipers. The dura samples were then transported to the mechanical testing device. The ends of each sample were removed, and thickness of these samples was measured optically with a calibrated, motorized microscope stage (Prior Scientific, Inc., Rockland, MD) by focusing on the bottom surface of the sample, recording the stage position in microns, and then focusing on the top surface of the sample and again recording stage position in microns. Spinal dura samples were ~80 mm thick and ~1–1.5 mm in width. The average cross-sectional area was 0.138 ± 0.025 mm^2.

Dura from the rat brain was harvested from Long-Evans hooded rats (77 ± 5 days). Animals were euthanized as described above and decapitated. The skull was removed to expose the dura. The dura mater covering the brain was demarcated *in situ* into 4 mm segments with an indelible marker (Fig. 1B). The dura was then removed and placed in PBS prior to testing. Typically, four samples were harvested per animal. Length and width measurements were taken at the central 8 mm with calipers. The dura samples were then transported to the mechanical testing device. Parts of the dura not used for mechanical testing were removed for thickness measurements. Cranial dura samples were ~80 mm thick and ~1.5–2.5 mm in width. The average cross-sectional area was 0.187 ± 0.032 mm^2. All

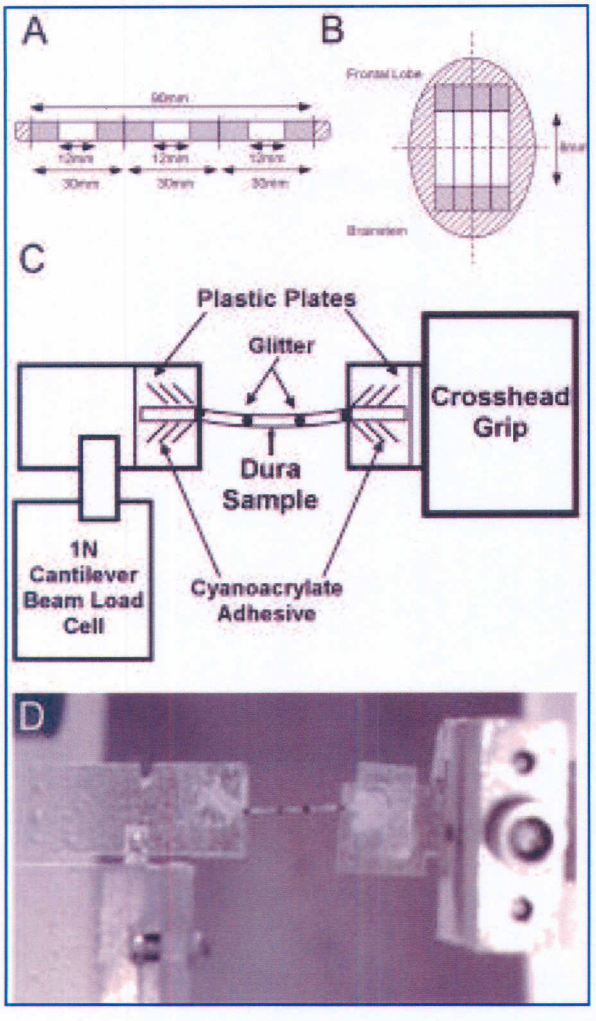

FIG. 1. Description of samples and testing setup. (**A**) For spinal samples, the dura was marked *in vivo* into 30-mm segments, and the central 12 mm of each 30-mm segmented was also marked. The remaining areas (gray) were used for gripping, and the hashed areas were used for thickness measurements. (**B**) For cranial dura, 8-mm-long samples were similarly marked. (**C**) The dura samples were secured by gluing the ends of the sample to plastic plates attached to either the load cell or the actuator. Small pieces of reflective plastic (glitter) were used to track tissue displacement. (**D**) A sample in the setup.

experimental procedures involving animals were approved by the Rutgers University Animal Care and Facilities Committee (IACUC 02-015).

Mechanical Testing

Spinal and cranial dura samples were tested in uniaxial tension using a Bose/Enduratec ELF 3200 (Bose Corporation, Eden Prairie, MN) with a 1-N cantilever load cell (Measurement Specialties, Hampton, VA). Separate, thin plastic plates were secured to the actuator (via compression grips) and to the load cell (via a rigid bolt), which was calibrated with the plate in place. The two plastic plates were then positioned to be 10 mm apart. The ends of the dura sample were placed on the plastic plate and covered with a cyanoacrylate adhesive (Krazy Glue, Columbus, OH), and two additional, separate plastic plates were placed on top of the dura on each grip, sandwiching each end of the dura between the plastic plates and creating plastic-plastic as well as dura-plastic adhesion to prevent any slipping of the dura relative to the plastic plate. Small pieces of reflective plastic (glitter) were placed on each dura sample to measure strain uniformity. A schematic of the setup and an image of a loaded sample are provided in Figure 1C,D. During the entire process, the dura samples were kept well hydrated by an ultrasonic humidifier (Wachsmuth & Krogmann, Elk Grove Village, IL) positioned under the sample. Once engaged in the grips, the samples were slowly stretched back to the original *in vivo* length of 12 mm for the spinal dura or 8 mm for the cranial dura and allowed to equilibrate for several minutes. All mechanical tests were done within 2 h of sacrifice to reduce tissue breakdown, since it was previously reported that post-mortem time can significantly affect the mechanical properties of biological tissues (Galford and McElhaney, 1970; Bilston and Thibault, 1996).

Samples of cranial and spinal dura mater were tested in uniaxial tension at one of two rates. Some samples ($n = 8$ for spinal dura, $n = 8$ for cranial dura) were subjected to rapid extension to 10% stretch at a strain rate of 19.4 sec^{-1} and held for 10 sec. Although the total time to reach peak displacement was ~9–10 msec, the linear portion accounted for ~95% of the curve, with the remaining contributions from the brief period of time required to ramp the actuator up to speed or back to zero velocity, and the strain rate was estimated from the slope of the curve. The remaining samples ($n = 15$ for spinal dura, $n = 8$ for cranial dura) were loaded at a strain rate of 0.0014 sec^{-1} until failure. For these tests, dura samples were preconditioned at a strain rate of 0.0014 sec^{-1} to 10% strain. It was determined that four preconditioning cycles were necessary before stress-strain equilibrium was reached for spinal and cranial dura samples, after which these samples were uniaxially loaded until failure. (The high strain rates and relatively large extension precluded cyclic preconditioning of the samples for high strain rate tests.) Load and displacement were recorded for the duration of the test. Images were documented every 2 mm of displacement using a digital camera (Nikon Coolpix S500, Melville, NY) to assess the uni-

formity of strain from the glitter using image analysis (Microsuite Analysis Software, Olympic Scientific, Mellville, NY). Specifically, the strain in the dura was compared among pairs of markers, using the ends of the grips as additional points, by determining stretch ratio in each section and normalizing by the overall stretch ratio.

Constitutive Modeling of the Rat Dura

The dura mater was modeled as a hyperelastic-linearly viscoelastic continuum solid. At very fast rates (i.e., instantaneous) and very slow rates (i.e., quasistatic), the model assumes hyperelastic behavior. An Ogden form of the hyperelastic strain energy potential function, W, which has previously been used to model both spinal cord and brain tissue (Bilston and Thibault, 1996; Miller and Chinzei, 2002), was used to model the elastic behavior of the dura:

$$W = \sum_{i=1}^{M} \frac{2G_i}{\alpha_i^2} \left(\lambda_1^{\alpha i} + \lambda_2^{\alpha i} + \lambda_3^{\alpha i} - 3\right) \quad (1)$$

where λ_i are the principal stretches, N is the complexity of the law, which is material dependent, and G_i and α_i are material-dependent parameters. For simple, uniaxial tension, assuming incompressibility, the relationship between nominal stress and stretch ratio for an Ogden material is:

$$\sigma = \sum_{i=1}^{M} \frac{2G_i}{\alpha_i} \left(\lambda_1^{\alpha_i - 1} - \lambda_1^{-0.5\alpha_i - 1}\right) \quad (2)$$

Volumetric changes due to thermal expansion are ignored. The instantaneous shear modulus is therefore given by:

$$G_0 = \sum_{i=1}^{M} G_i \quad (3)$$

Based on the results, a one term Ogden function ($M = 1$) was used.

The viscoelastic portion of the material laws was described with a Prony series exponential decay:

$$G_R(t) = G_0\left[1 - \sum_{k=1}^{N} g_k \left(1 - e^{-t/\tau k}\right)\right] \quad (4)$$

where the instantaneous shear modulus is multiplied by a normalized function that includes relative relaxations, g_k, at characteristic time constants, τ_k. The quasi-static shear modulus can then be related to the instantaneous modulus by:

$$G_\infty = G_0\left(1 - \sum_{k=1}^{N} g_k\right) \quad (5)$$

The slow rate response of the dura was fit with the Ogden hyperelastic representation of the quasi-static shear moduli based on Eq. 2 (Kaleidagraph, Synergy Software, Reading, PA). Viscoelastic time constants were determined by normalizing the relaxation portion of the stress vs. time curves of the high rate tests and fitting the curves to the bracketed term of Eq. 4 (Bilston and Thibault, 1996; Miller and Chinzei, 2002; Prange and Margulies, 2002) (SPSS 15.0, Chicago, IL), and the two are combined to identify the instantaneous shear moduli via Eq. 5. Based on the results, a 4-term Prony series was used ($N = 4$).

Statistical Analysis

Descriptive statistics were taken for all experimental results of the stress relaxation data, as well as the stress-strain data. Ogden and Prony Series parameters, as well as failure properties, were compared statistically between the cranial and spinal dura mater with one-way analysis of variance (ANOVA; $P < 0.05$).

Polarized Light Microscopy

Alignment of fibers in the dura mater was initially assessed qualitatively with polarized light microscopy. Long-Evans hooded rats (77 days old) were euthanized with a lethal dose of sodium pentobarbital (65 mg/kg), exsanguinated with 200 mL of heparinized saline, and perfused transcardially with 10% formalin. The spinal and cranial dura were removed and stored in 10% formalin for 2 h. Dura samples were then mounted on charged glass slides (Superfrost Plus, Fisher Scientific, Pittsburgh, PA) and placed on the microscope stage between a linear polarizer and a linear analyzer oriented as 'cross-polars' with axes of polarization 90° apart. The dura samples were rotated between 0° and 180°. Separate mosaic images for the cranial and spinal dura were generated via a Hamamatsu ORCA CCD camera (Bridgewater, NJ) using computer controlled microscopy (Olympus IX81; Olympus America, Center Valley, PA) to assess anisotropy in the tissue fibers.

Histology

Dura structure and composition were visualized with Masson's Tri-chrome for collagen or Verhoeff's Van Gieson stain for collagen and elastic tissue. Dura samples were harvested from transcardially perfused animals as described above and stored in 10% formalin for 2 h. Samples were then placed in 20% sucrose solution overnight for cryoprotection. Dura samples were sectioned horizontally into 20 μm sections with a cryostat (ThermoShandon, Pittsburgh, PA). Sections were mounted on charged glass slides (Superfrost Plus, Fisher, Pittsburgh, PA) and stained for elastin, collagen, and cell nuclei using Sigma Accustain Elastic Stain kit or Tri-Chrome kit (Sigma Aldrich, St. Louis, MO) in accordance

with the manufacturer's specifications. Samples were coverslipped using DPX histology mounting medium (Sigma), and brightfield images were captured with an upright microscope (Carl Zeiss Microimaging, Inc., Thornwood, NY).

RESULTS

Low Strain Rate Stress-Strain Response

Both cranial and spinal dura mater demonstrated non-linear stress-strain behavior typical of collagenous soft tissues when tested to failure in uniaxial tension at slow rates (0.0014 sec^{-1}). In general, both tissue types generated peak forces between 0.15 and 0.6 N, though the response of spinal dura was more variable than cranial dura, especially during the elastic portion of the curve, where the onset of the non-linear portion shifted considerably. Consistent behavior was not observed past the perceived yield point for either cranial or spinal dura, which was estimated by fitting a line to the linear portion of the upswing of the stress-stretch curve, and identifying where the response deviated from this line via either a drop in stress or a gradual decrease in the slope. Some samples failed completely soon after yielding, some continued to carry increasing load, albeit at lower apparent stiffness than during the elastic portion, and some demonstrated multiple drops and recoveries in the stress-stretch response. We note that the samples did not yield in the traditional sense of the onset of plastic deformation, but rather likely demonstrated failure of individual matrix fibers and a subsequent redistribution of load to the remaining fibers. Digital image analysis (Microsuite Analysis Software) was used to assess the uniformity of strain in the dura during uniaxial tensile testing. The stretch ratio in the dura was compared among three pairs of markers, using the grips as additional points. No significant differences were detected for the stretch from the left grip to the first marker, the first to the second marker, or the second marker to right grip within the elastic region. During this time, the normalized stretch (stretch in a section divided by overall stretch) showed no discernable pattern and ranged from 0.99 to 1.01.

For each curve, the elastic portion was identified by fitting the linear portion of the stress-stretch curve and determining where the curve began to deviate from this line (Fig. 2). The average yield stress and stretch at yield (±SD) was lower for cranial dura (1.27 ± 0.66 MPa at $\lambda = 1.13 \pm 0.01$) than spinal dura (2.14 ± 1.56 MPa at $\lambda = 1.24 \pm 0.16$), but neither difference was significant ($p = 0.148$ and $p = 0.085$, respectively). The average ultimate tensile stress for spinal dura mater was 2.91 ± 1.30 MPa at an average stretch ratio of 1.43 ± 0.183, and

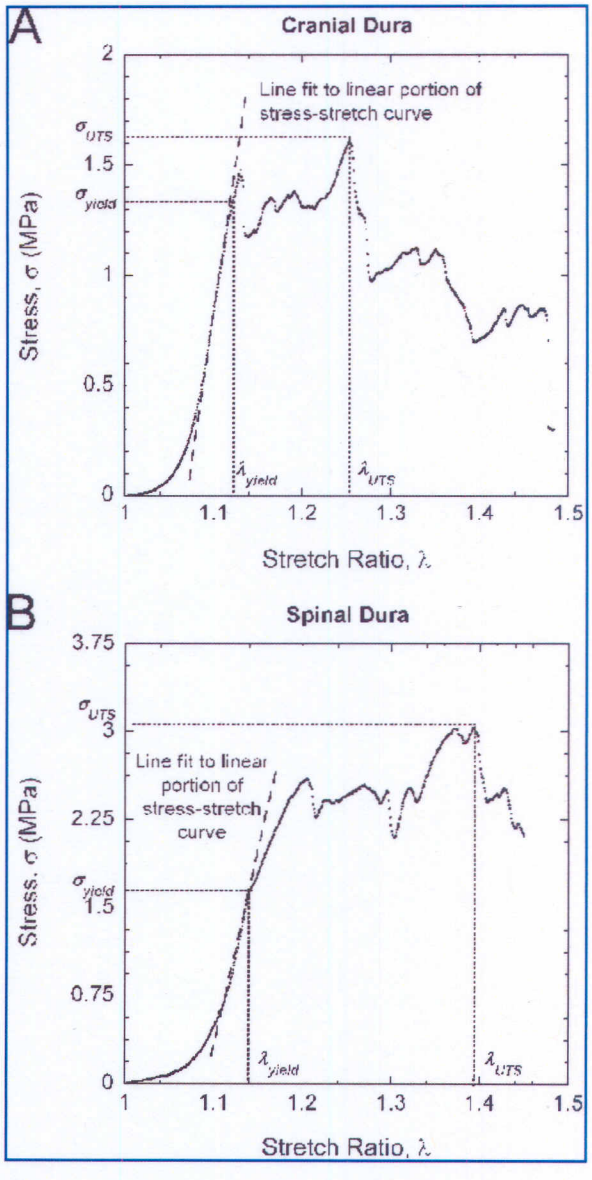

FIG. 2. Representative stress-stretch curves for cranial (**A**) and spinal dura (**B**). Dura samples were loaded in uniaxial tension at 0.014 sec^{-1} until failure. Both spinal and cranial samples demonstrated non-linear stiffening consistent with load-bearing soft tissues. The behavior following yielding/microfracture was highly variable. The "yield stress" (σ_y) was identified as the point where the stress-stretch response began to deviate from the linear portion of the response. The ultimate tensile stress (σ_{UTS}) was identified as the maximum tension achieved in an experiment. The stretch at yield stress (λ_y) and at ultimate tensile stress (λ_{UTS}) were identified accordingly. In general, cranial samples demonstrated more acute non-linear stiffening at lower stretch ratios than spinal cord samples.

TABLE 1. CONSTANTS OF THE OGDEN HYPERPLASTIC MODEL FOR SPINAL AND CRANIAL DURA

$$\sigma = \frac{2G}{\alpha}(\lambda_1^{\alpha-1} - \lambda_1^{-0.5\alpha-1})$$

Parameter	*Spinal dura, Average value ±SD*	*Cranial dura, Average value ±SD*	p-*value*
G (MPa)	1.20 ± 0.79	0.42 ± 0.19	0.012*
α	16.2 ± 9.74	32.9 ± 6.65	0.002*
R^2 for Ogden Fit	0.98	0.98	—
Yield Stress (MPa)	2.14 ± 1.56	1.27 ± 0.66	0.148
Stretch at Yield	1.24 ± 0.16	1.13 ± 0.01	0.085
Ultimate Tensile Strength (MPa)	2.91 ± 1.30	2.49 ± 2.03	0.55
Stretch at UTS	1.43 ± 0.183	1.39 ± 0.133	0.53

*Significant difference observed between cranial and spinal dura, ANOVA, $p < 0.05$.

the average ultimate tensile stress for cranial dura mater was 2.49 ± 2.03 MPa at an average stretch ratio of 1.39 ± 0.133, which were also not significantly different ($p = 0.55$ and $p = 0.57$, respectively).

The elastic portion of each stress-stretch ratio curve was fit to a one-term Ogden hyperelastic constitutive model (Eq. 2 with $M = 1$), which sufficiently captured the stress-strain behavior, to identify the material parameters for the spinal and cranial dura (Table 1). The stiffness, G of spinal dura was significantly greater than cranial dura ($p = 0.012$), whereas α, which generally introduces the non-linearity into the constitutive law, was significantly greater for cranial dura ($p = 0.0002$). The average Ogden formulations for cranial and spinal dura are plotted in Figure 3.

Stress-Relaxation Response of the Rat Spinal Dura

The viscoelastic response of the dura was assessed via stress relaxation by loading samples to 10% stretch at a strain rate of 19.4 sec^{-1} and holding at that stretch for 10 sec, during which time both cranial and spinal dura mater exhibited significant relaxation (spinal dura ~64%; cranial dura ~69%). A representative plot of the first 50 msec of programmed displacement, actual displacement, and measured force is shown in Figure 4. The mean stress relaxation responses for the rat spinal and cranial dura over the entire loading history are shown in Figure 5. To identify time constants from the stress-relaxation data that are appropriate for biomechanics studies at different time scales, the decay function was fit with a four-term Prony series decay function, which captured the early time constants necessary for modeling traumatic loading conditions, while still preserving the full decay time history without the cost of the accuracy of the shorter time constants (Table 2). The individual constants from the Prony series from cranial and spinal dura mater were compared with one-way ANOVA, and the results indicated that the dura from the brain relaxes more quickly than that from the spinal cord. The first two time constants—τ_1 and τ_2—were significantly different between the spinal and cranial dura ($p < 0.007$), while the last two time constants—τ_3 and τ_4—were not significantly dif-

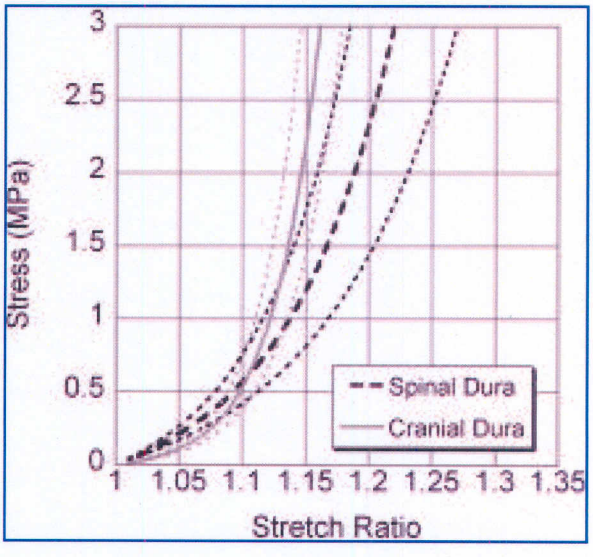

FIG. 3. Ogden hyperelastic material laws derived from average properties (± standard error) for spinal and cranial dura. The yield point from each stress-stretch curve was identified by a deviation from the linear portion of the curve. The "elastic" portion of each curve was fit to a one-term Ogden hyperelastic model to determine the stiffness parameter, G, and the exponent α, from Eq. 1, and the average of these parameters was used for the material model. Cranial dura demonstrates a lower stiffness at low stretch levels, but increases non-linearly at a greater rate than spinal dura.

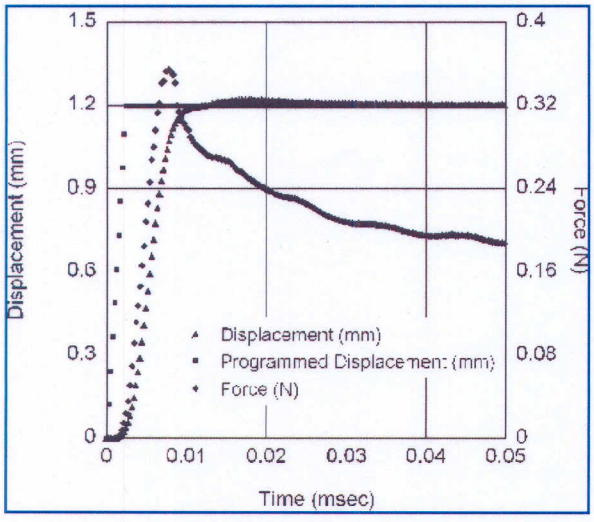

FIG. 4. Representative plot of the loading portion and first 50 msec of relaxation during viscoelastic testing. To achieve the rapid actuator displacement (triangles), the testing device was prescribed an even faster ramp (squares). The strain rate was estimated from the linear portion of the displacement ramp, which accounted for ~95% of the applied displacement. The force peak leads the displacement peak, and then relaxes significantly during the first 50 msec.

ferent ($p > 0.1$). All four relative stress relaxation constants—g_1, g_2, g_3, and g_4—were significantly different between the spinal and cranial dura ($p < 0.002$). However, the net relaxation (sum g_1-g_4) was not significant ($p = 0.102$).

Polarized Light Microscopy and Elastic Stain Histology

Whole rat spinal and cranial dura samples were interrogated with polarized light to visualize anisotropy in the fibrillar matrix. Spinal dura samples demonstrated substantial alignment; when samples were placed coincident with the axis of polarization, nearly all light was extinguished (Fig. 6A). However, when the sample was oriented at ~45° between polarizer and analyzer, the intensity increased significantly (Fig. 6B), indicating alignment in the axial direction (though alignment in the transverse direction is also possible). Unlike spinal dura samples, dura mater from the rat brain exhibited minimal alignment. Under cross-polars, intensity was moderate when samples were placed coincident with the axis of polarization (Fig. 6C). The pattern of intensity when the sample was rotated to ~45° changed, but the overall intensity remained approximately the same (Fig. 6D). The average pixel intensity (on a scale of 0–255) of the images in Figure 6 was calculated with Olympus Microsuite Image Analysis Software. The average intensity rose from 24.6 to 84.8 when the spinal sample was rotated off-axis, whereas the average intensity of the cranial sample rose minimally from 44.3 to 50.4.

Histology

Verhoeff's Van Gieson Staining for collagen and elastin confirmed that the prevailing orientation of spinal dura was axial. The spinal dura in Figure 7A shows a prevalence of cell nuclei that are preferentially aligned along the collagen and elastin. Collagen in this section is organized in large bundles. Figure 7B reveals a considerable amount of elastin as well as collagen in the axially oriented matrix. Cranial dura samples stained with Verhoeff's Van Gieson stain showed random orientation of collagen fibers and fewer elastic fibers (Fig. 7C). Trichrome staining of collagen revealed an interwoven meshwork of fibers in cranial dura (Fig. 7D).

DISCUSSION

The primary purpose of this work was to describe the material properties of dura mater harvested from the rat brain and spinal cord. Rat models of TBI and SCI have been invaluable in identifying the pathological sequelae following trauma and in evaluating therapeutic means of

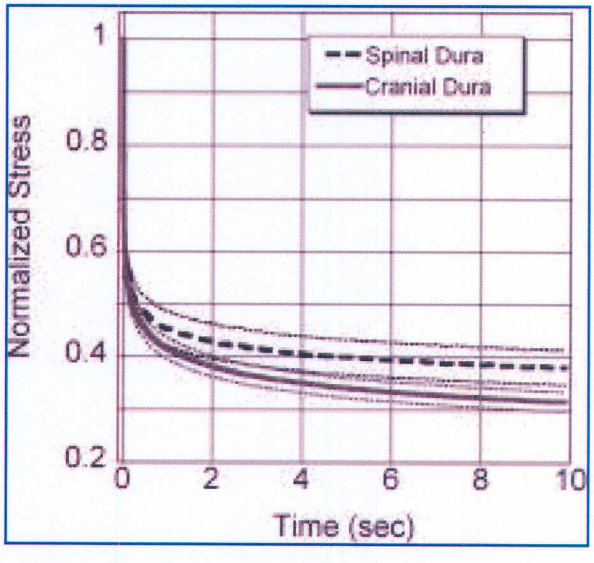

FIG. 5. Mean relaxation response (± standard error) of spinal and cranial dura. Dura samples were loaded to 10% stretch at a rate of 19.4 sec^{-1} and held at that stretch for 10 sec. The resultant stress was normalized by peak stress and fit to a four-term Prony series exponential decay, which is summarized in Table 2.

Table 2. Summary of Relaxation Constants for Spinal and Cranial Dura

$$G_0 = G_\infty\left[1 - g_1\left(1 - \exp\left(\frac{-t}{\tau_1}\right)\right) - g_2\left(1 - \exp\left(\frac{-t}{\tau_2}\right)\right) - g_3\left(1 - \exp\left(\frac{-t}{\tau_3}\right)\right) - g_4\left(1 - \exp\left(\frac{-t}{\tau_4}\right)\right)\right]$$

	Average value (SD)		
Constant	*Spinal dura*	*Cranial dura*	p-*value*
g_1	0.329 (0.50)	0.240 (0.053)	0.004*
τ_1	0.009 (0.002)	0.005 (0.002)	0.007*
g_2	0.128 (0.030)	0.213 (0.027)	0.0001*
τ_2	0.0081 (0.026)	0.044 (0.012)	0.003*
g_3	0.086 (0.021)	0.118 (0.011)	0.002*
τ_3	0.564 (0.190)	0.474 (0.071)	0.228
g_4	0.086 (0.013)	0.122 (0.019)	0.001*
τ_4	4.69 (1.202)	3.99 (0.490)	0.152
G_∞/G_0	0.371 (0.089)	0.307 (0.054)	0.102
R^2	0.99	0.99	—

*Significant differences observed between cranial and spinal dura, ANOVA, $p < 0.05$.

intervention, and often deliver the mechanical insult across the intact dura mater. Thus, to evaluate the tissue biomechanics associated with these models, the contribution of the dura mater to the overall mechanical response must be included. The dura from both rat brain and rat spinal cord were modeled effectively with an Ogden hyperelastic-linear viscoelastic constitutive law. The stiffness parameter from the Ogden law for the cranial dura was lower than spinal dura, and the non-linear stiffening with increasing stretch was more pronounced for cranial dura than spinal dura. Analysis of relaxation data following high strain rate uniaxial loading indicated that, although the total relaxation of the samples was similar, the dura from the brain relaxed faster than that from the spinal cord.

As with the dura mater in other species, the rat dura mater is significantly stiffer than the CNS tissue it surrounds, which points to its protective role. For instance, Gefen et al. report that the in situ quasistatic shear modulus of rat brain is 0.1–1 kPa, depending on the age of the tissue and whether it was preconditioned. By comparison, we found the rat cranial dura has a modulus on the order of 1 MPa. Similarly, the rat spinal dura has a modulus in tension that is two orders of magnitude greater than the stiffness of rat spinal cord (Fiford and Bilston, 2005). The dura, therefore, will contribute significantly to the overall mechanical response of the brain and/or spinal cord to traumatic loading and may absorb a large percentage of the kinetic energy, especially in models where the insult is delivered directly to the dura. As such, the data described herein is valuable as input material parameters for simulations of rat models of TBI and SCI.

The differences in Ogden model properties of rat cranial and spinal dura mater may be linked to their mechanical functions. Whereas the brain is encased in a rigid skull, the enhanced mobility and flexibility of the spine requires the structures of the spinal cord to routinely experience mechanical loading during movement. For instance, MRI studies have shown that the human cervical spinal cord can experience 6–10% strain during flexion (Yuan et al., 1998). Thus, the extended lag phase in spinal dura can allow routine movement with less stress generation, which is not necessary in the cranial dura mater. The stress-strain behavior of cranial dura may therefore provide some compliance for smaller variations in CSF pressure while restricting expansion for larger increases.

Previous reports, collectively, have demonstrated that the properties of excised brain tissue are well correlated to those *in vivo,* provided that the tests on excised tissue are performed soon after sacrifice (Gefen et al., 2003;

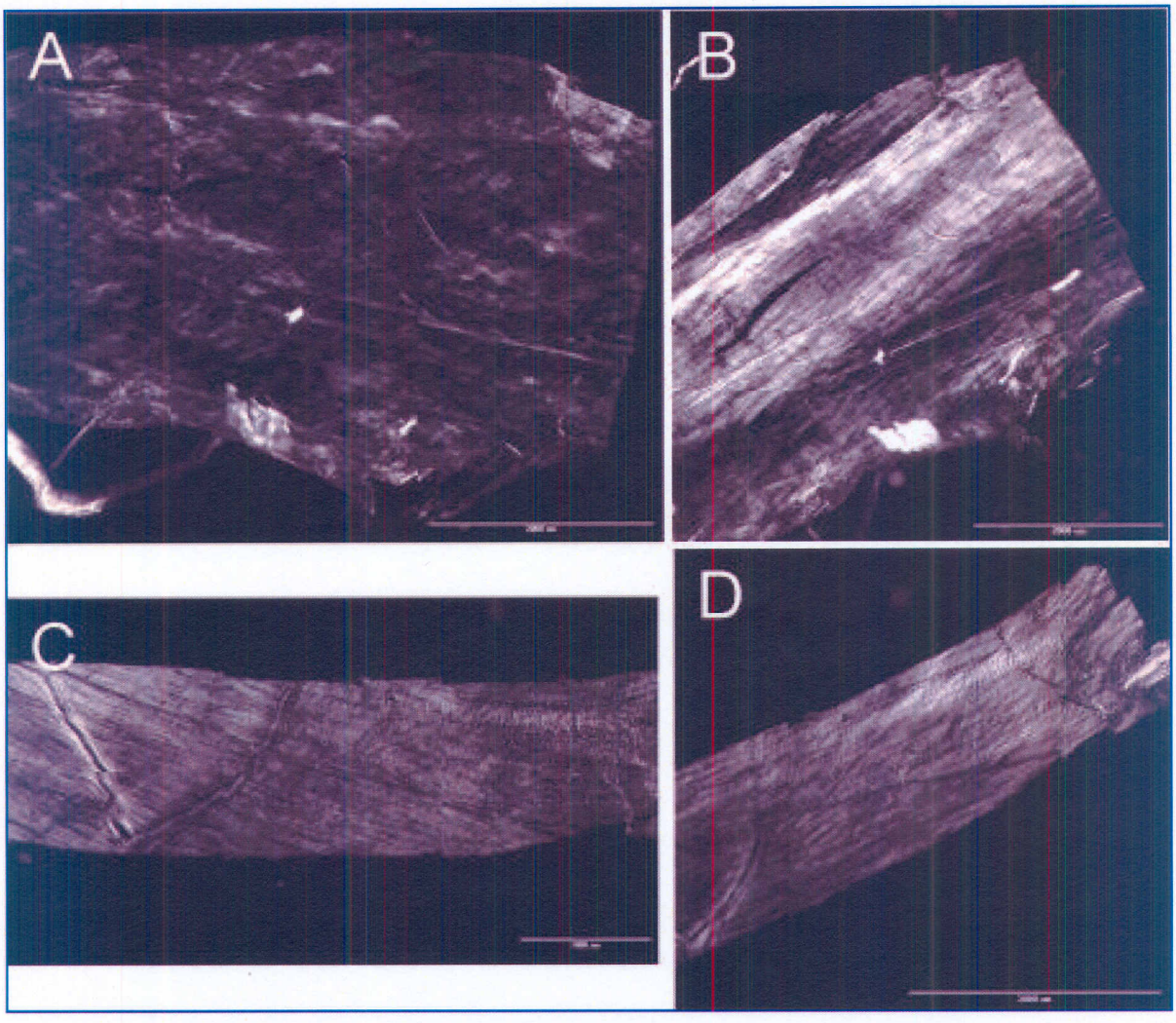

FIG. 6. Assessment of alignment with polarized light microscopy. Whole-thickness dura samples were interrogated with linearly polarized light, which was subsequently passed through a second linear polarizer oriented 90° from the first polarizer to analyze the orientation. (**A**) Spinal dura samples oriented with the long axis of the sample coincident with the axis of polarization extinguished nearly all of the light (average intensity for this image = 24.6 on an eight-gray, 0–255 scale). (**B**) A substantial increase in intensity was observed when the sample was rotated ~45°, indicating that the fibers comprising the spinal dura are oriented axially (average intensity = 84.8). (**C**) Cranial samples placed with the long axis of the sample coincident with the axis of polarization an inhomgeneous intensity field of moderate intensity (average intensity = 44.3). (**D**) Upon rotating the sample, a redistribution of intensity is observed, but the increase in overall intensity was small (average intensity = 50.4).

Gefen and Margulies, 2004). In this study, all samples were tested within 2 h of euthanasia and harvest. In addition, both cranial and spinal dura were very thin (~80 μm) and dehydrated quickly when exposed to air. To avoid the effects of dehydration, our samples were immersed in PBS during sample preparation, and a constant mist was provided during the actual mechanical testing. In preliminary experiments, we found that the stress-strain behavior and strain uniformity of the tissue was much more consistent when tissue was supplied with a constant, extremely fine mist via the ultrasonic humidifier versus intermittent spray with saline (data not shown). Additionally, when not in solution, the dura tended to coil and fold onto itself. Special care was taken to avoid overlapping of the dura while placing the sample onto the grips, which again resulted in improved consistency in the results. Recording the displacement along the length of the samples via fiduciary markers provided

a means of evaluating strain uniformity and, additionally, a measure of the general quality of individual experiments. In general, the behavior in the elastic region was more consistent with cranial dura. Preliminary experiments demonstrated that the range and variability of spinal samples was the same in different regions (cervical, thoracic, lumbar—data not shown), and these samples were lumped together for the analysis. We also did not attempt to remove the arachnoid layer from the inferior side of the dura mater, for fear of introducing structural damage that would confound the mechanical testing results. Other studies also report the structure and/or mechanical properties for human and bovine dura with the arachnoid in tact (Runza et al., 1999) or with a simple excision procedure of the dura, from which it is assumed that the arachnoid remains with the tissue (Patin et al., 1993; Hamann et al., 1998). A recent report indicates that the cranial pia-arachnoid complex does provide mechanical protection for brain tissue, based on the properties of bovine tissue, and we presume it would provide similar protection for spinal cord tissue (Jin et al., 2006). However, the relative thickness of the dura-to-arachnoid (Vandenabeele et al., 1996; Runza et al., 1999)and the relative lack of organized extracellular matrix in the arachnoid (Vandenabeele et al., 1996) suggests that the arachnoid would contribute minimally to the properties examined herein. We are developing techniques to separate the two tissues, but the rat dura is thinner than other species studied, and reproducibly isolating the tissues is challenging.

The general, non-linear stress-strain response of rat dura mater is consistent with other collagenous, load bearing soft tissues, such as ligaments, tendons, and skin. In vivo, fibers from human dura tend to have an inherent undulated nature and are potentially aligned randomly (Frisen et al., 1969). During the initial stages of uniaxial tensile loading, those fibers begin to orient themselves in the direction of loading, straighten, and stretch, which leads to an initial compliance and lag in the stress (Viidik, 1968; Frisen et al., 1969). As strain increases, the fibers further align and take on more load, which leads to a non-linear increase in stiffness (Viidik, 1968; Frisen et al., 1969; Bilston and Thibault, 1996; Fiford and Bilston, 2005). Additionally, the dura has a significant number of elastin fibers, which are believed to contribute to the low-strain, toe-region of the stress-strain curve for soft tissues (Park, 1984).

The differences in material behavior prompted us to preliminarily examine the structure and composition of the tissues. Polarized light microscopy indicated that the microstructure of spinal dura was significantly aligned, whereas cranial dura was more randomly oriented. Histological staining also indicated that the spinal dura was aligned along the axis of the spinal cord, but that orientation of the cranial dura was inhomogeneous and often random. The histology also suggested that rat spinal dura maintains greater elastin content than cranial dura. The alignment of spinal dura was aligned in the direction of uniaxial testing, but also maintained greater elastin content. By comparison, the cranial dura showed a mesh-like structure and a lower elastin-content. The data suggests that transition from elastin to collagen loading is a strong factor in the non-linear stiffening of spinal dura, whereas rotation and alignment of collagen fibers in the direction of stretch is responsible for the non-linear stiffening in cranial dura. These results are qualitative, and a detailed, quantitative assessment of the structural organization via electron microscopy, small angle light scattering (SALS), or associated technique, as well as the composition via quantitative microscopy and digestive assays is necessary and warranted to develop a true structure-function relationship for these tissues.

The alignment we observed in the spinal dura generally matches that found in human samples. Histology and scanning electron microscopy studies have shown that collagen fibers in the human lumbar dura mater demonstrated a preferential longitudinal orientation, which imparted transversely isotropic material properties. Stiffness in the direction of the fibers was ~5–10 times the stiffness transverse to the fibers (Patin et al., 1993). In the present study, we only examined the mechanical properties of dura in the longitudinal/sagittal direction, primarily because the short width of the spinal samples precluded effective testing with our mechanical testing system in the transverse/coronal direction, and we are thus limited to an isotropic material law, when an anisotropic law is warranted, particularly for the spinal dura.

Unlike human lumbar dura, histological staining of canine lumbar dura mater showed no preferred longitudinal orientation, but instead an increased number of transverse fibers, and an associated absence of directional properties (Patin et al., 1993). Additionally, bovine lumbar dura tested in uniaxial tension in the longitudinal direction demonstrated a much longer "lag" portion compared to human lumbar dura tested parallel (Runza et al., 1999). Together, these data indicate there can be considerable species-to-species variation in the fundamental mechanical behavior of the dura mater, and it has been suggested that differences observed were partly due to the supine vs. upright nature of the species, as well as the associated lack of gravity-induced CSF pressure (Patin et al., 1993). The rat, of course, is a supine animal, yet rat spinal dura clearly demonstrated longitudinal alignment. Increased flexibility of the rat, coupled with a diminished hoop stress because of the smaller radius of the spinal

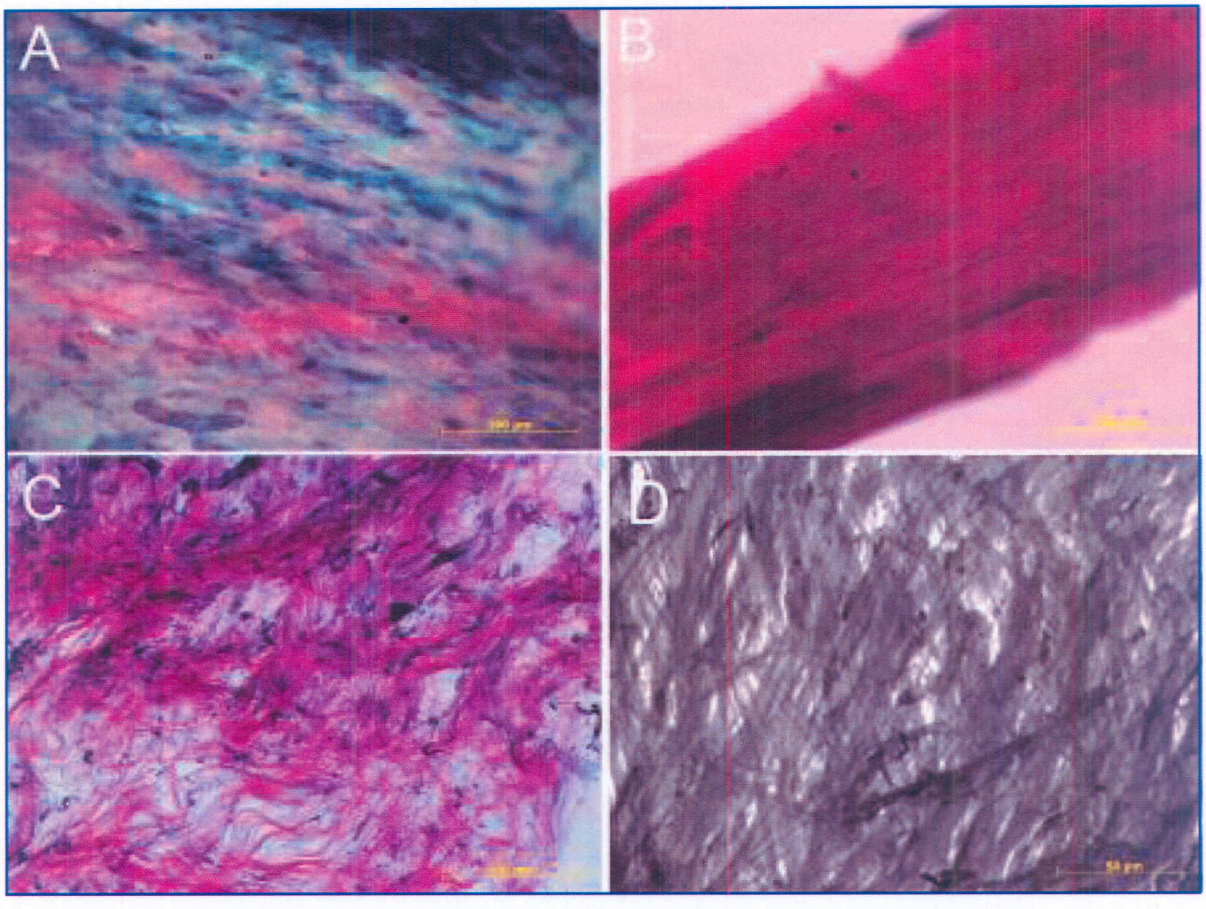

FIG. 7. Histological staining of spinal (**A,B**) and cranial (**C,D**) dura. Verhoeff's Van Gieson staining (**A–C**) showed that spinal and cranial dura both include collagen and elastin, though the elastin content appeared to be greater in spinal samples. Spinal dura fibers appeared to be aligned axially (B), and induced orientation of cell nuclei in a cell-dense layer of the dura (A). In some areas, cranial dura fibers tended to appear randomly oriented and wavy (C), while in other areas, a criss-cross, hatched appearance was apparent (Tri-chrome staining; D). (Color image is available online at www.liebertpub.com/jon)

cord, and, therefore, less need for circumferential reinforcement, may explain the preferred axial alignment in this species versus other, larger supine animals.

The alignment we observed in the rat cranial dura generally matched that from human cranial dura. McGarvey et al. (1984) reported that the cranial dura fibers showed some local orientation, but often changed direction within a 5-mm distance. They tested the cranial dura both longitudinally and transversely and determined that the cranial dura had an average stiffness of approximately 60 MPa. Van Noort et al. (1981) performed tensile loading tests on human cranial dura and determined an average stiffness of 30 MPa, but also noted that many of the samples were from cadavers older than 50 years, which could contribute to poor quality dura. They also determined through histology that at short distances, there are indications of preferred fiber orientation. Hamann et al. (1998) performed an in depth quantification of fibers orientation using SALS in the human cranial dura and determined that the fibers had multiple preferred orientations except in the temporal region. Thus, it appears that dura mater from the brain may demonstrate anisotropic properties locally but tend towards isotropic properties in bulk measurements. The primary stresses experienced by the cranial dura are from CSF pressure, which would induce a roughly uniform membrane tension throughout the dura, with local variations due to anatomical/geometric factors that could lead to the local variations in alignment.

We performed stress relaxation tests at a significantly higher strain rate ($\sim$20 sec^{-1}) than those used in published studies of dura material properties of any species.

High strain rate tests are necessary to capture the response of tissue in a regime that is relevant for neurotrauma clinically, as well as to emulate the strain rates applied in many *in vivo* SCI and TBI models (Dixon et al., 1987; Stokes et al., 1992; Meaney et al., 1994; Young, 2002). Previously, Patin et al. (1993) tested human lumbar dura in both longitudinal and transverse directions to a strain that corresponded to half failure at a rate of 10 cm/min. They noted that 15–33% of the stress relaxed in 24 sec, but unlike failure testing, stress relaxation testing showed no mechanical directionality. McGarvey et al. (1984) performed stress relaxation tests between 5% and 500% min^{-1} on human cranial dura and showed that, on average, approximately 20% of the stress relaxed in 1000 sec. We found cranial and spinal dura mater demonstrated more than 60% relaxation when strained at the higher rates. This relaxation is substantially greater than previous reports, which undoubtedly is related to the generation of greater stresses at higher rates, essentially supplying more stress to relax than had been done in the previous studies.

We fit the relaxation data to a four-term Prony series exponential decay. The four-term Prony series decay function allowed an accurate determination of short ($<$100 msec), intermediate (100 msec to 1 sec), and long ($>$1 sec) time constants, and provides a robust material determination for different biomechanical studies and simulations. Traumatic injury studies clearly call for accurate assessment of short time constants, and splitting the relaxation into four terms resulted in time constants on the same order as loading rates experienced in trauma and in models of TBI and SCI. However, there are other instances where loading of brain and spinal cord structures occurs over a longer time period and the mechanics may be more appropriately modeled with the intermediate and long time constants, and possibly constants determined from longer hold periods than the 10 sec employed herein, although the majority of relaxation had already occurred. Robotic and virtual surgeries (Federspil et al., 2003; Spicer et al., 2004), where the dynamic loads on the spinal and dura are within or just above physiological levels, chronic cord compression syndromes, such as syringomyelia (Loth et al., 2001; Carpenter et al., 2003) or hydrocephalus (Taylor and Miller, 2004; Linninger et al., 2007) that result in an increase in CSF pressure, or increased pressure from a myleoma, sarcoma, or other malignancies, are more appropriately modeled with longer hold times.

Whereas no significant differences were observed between the total relaxation of cranial and spinal dura, the distribution of relaxation among the four terms in the Prony series was different. Cranial dura had significantly shorter time constants for the first two terms than the spinal cord (5 and 44 msec, vs. 9 and 81 msec). The first two terms contributed approximately equally to the total relaxation for cranial dura (~24% vs. 21%), whereas the spinal dura experienced greater relaxation over the first time constant than the second one (33% vs. 13%). Together, the two terms accounted for 45% and 46% of the total stress, but the cranial dura relaxed nearly twice as fast. The cranial dura also demonstrated significantly more relaxation at later time constants than the spinal dura (3rd and 4th term), though there were no significant differences in the time constants, themselves. A detailed analysis of composition and structure-function behavior is likely necessary to identify the source of the differences in relaxation behavior between spinal and cranial dura mater.

However, for both tissues, relaxing the dura stiffness may allow relief of the circumferential/hoop stress generated by intracranial/intrathecal pressure by allowing some volume expansion, which may be especially significant for the cranial dura because of the larger radius. Additionally, relaxation in spinal dura is necessary to alleviate stresses during routine postural movements and extended times in flexion and extension. It is well known that fibroblasts, the chief cell type in dura mater, respond phenotypically to mechanical tension by altering their cytoskeleton and adhesion to the surrounding matrix and their synthesis of proteins and enzymes involved in matrix re-organization, including an increase in type I collagen synthesis, to appropriately adjust the tissue's properties. The large, cumulative relaxation in dura mater will also assist in shielding fibroblasts from these stresses to limit matrix remodeling of the tissue (Kessler et al., 2001; D'Addario et al., 2003; He et al., 2004; Petroll et al., 2004).

ACKNOWLEDGMENTS

Funding for these studies was provided by the National Center for Injury Prevention and Control at the Centers for Disease Control (R49CCR 221744-01) and a graduate fellowship to J.T.M. from the New Jersey Commission on Spinal Cord Research (04-2903-SCR-E-0).

REFERENCES

Berkowitz, E.D. (1998). Revealing America's welfare state. Rev. Am. Hist. **26,** 620–624.

Bilston, L.E., and Thibault, L.E. (1996). The mechanical properties of the human cervical spinal cord *in vitro*. Ann. Biomed. Eng. **24,** 67–74.

Carpenter, P.W., Berkouk, K., and Lucey, A.D. (2003). Pressure wave propagation in fluid-filled co-axial elastic tubes. Part 2: Mechanisms for the pathogenesis of syringomyelia. J. Biomech. Eng. **125,** 857–863.

D'addario, M., Arora, P.D., Ellen, R.P., and Mcculloch, C.A. (2003). Regulation of tension-induced mechanotranscriptional signals by the microtubule network in fibroblasts. J. Biol. Chem. **278,** 53090–53097.

Dixon, C.E., Lyeth, B.G., Povlishock, J.T., Findling, R.L., Hamm, R.J., Marmarou, A., Young, H.F., and Hayes, R.L. (1987). A fluid percussion model of experimental brain injury in the rat. J. Neurosurg. **67,** 110–119.

Federspil, P.A., Geisthoff, U.W., Henrich, D., and Plinkert, P.K. (2003). Development of the first force-controlled robot for otoneurosurgery. Laryngoscope **113,** 465–471.

Fiford, R.J., and Bilston, L.E. (2005). The mechanical properties of rat spinal cord in vitro. J. Biomech. **38,** 1509–1515.

Frisen, M., Magi, M., Sonnerup, I., and Viidik, A. (1969). Rheological analysis of soft collagenous tissue. Part I: Theoretical considerations. J. Biomech. **2,** 13–20.

Galford, J.E., and McElhaney, J.H. (1970). A viscoelastic study of scalp, brain, and dura. J. Biomech. **3,** 211–221.

Gefen, A., Gefen, N., Zhu, Q., Raghupathi, R., and Margulies, S.S. (2003). Age-dependent changes in material properties of the brain and braincase of the rat. J. Neurotrauma. **20,** 1163–1177.

Gefen, A., and Margulies, S.S. (2004). Are in vivo and in situ brain tissues mechanically similar? J. Biomech. **37,** 1339–1352.

Guertin, P.A. (2005). Paraplegic mice are leading to new advances in spinal cord injury research. Spinal Cord **43,** 459–461.

Hamann, M.C., Sacks, M.S., and Malinin, T.I. (1998). Quantification of the collagen fibre architecture of human cranial dura mater. J. Anat. **192,** 99–106.

He, Y., Macarak, E.J., Korostoff, J.M., and Howard, P.S. (2004). Compression and tension: differential effects on matrix accumulation by periodontal ligament fibroblasts *in vitro*. Connect. Tissue Res. **45,** 28–39.

Ichihara, K., Taguchi, T., Shimada, Y., Sakuramoto, I., Kawano, S., and Kawai, S. (2001). Gray matter of the bovine cervical spinal cord is mechanically more rigid and fragile than the white matter. J. Neurotrauma. **18,** 361–367.

Jin, X., Lee, J.B., Leung, L.Y., Zhang, L., Yang, K.H., and King, A.I. (2006). Biomechanical response of the bovine pia-arachnoid complex to tensile loading at varying strain-rates. Stapp Car Crash J. **50,** 637–649.

Kessler, D., Dethlefsen, S., Haase, I., Plomann, M., Hirche, F., Krieg, T., and Eckes, B. (2001). Fibroblasts in mechanically stressed collagen lattices assume a "synthetic" phenotype. J. Biol. Chem. **276,** 36575–36585.

Kraus, J.F., and McArthur, D.L. (1996). Epidemiologic aspects of brain injury. Neurol. Clin. **14,** 435–450.

Linninger, A.A., Xenos, M., Zhu, D.C., Somayaji, M.R., Kondapalli, S., and Penn, R.D. (2007). Cerebrospinal fluid flow in the normal and hydrocephalic human brain. IEEE Trans. Biomed. Eng. **54,** 291–302.

Loth, F., Yardimci, M.A., and Alperin, N. (2001). Hydrodynamic modeling of cerebrospinal fluid motion within the spinal cavity. J. Biomech. Eng. **123,** 71–79.

Mcgarvey, K.A., Lee, J.M., and Boughner, D.R. (1984). Mechanical suitability of glycerol-preserved human dura mater for construction of prosthetic cardiac valves. Biomaterials **5,** 109–117.

Meaney, D.F., Ross, D.T., Winkelstein, B.A., Brasko, J., Goldstein, D., Bilston, L.B., Thibault, L.E., and Gennarelli, T.A. (1994). Modification of the cortical impact model to produce axonal injury in the rat cerebral cortex. J. Neurotrauma. **11,** 599–612.

Miller, K., and Chinzei, K. (2002). Mechanical properties of brain tissue in tension. J. Biomech. **35,** 483–490.

Park, J.B. (1984). *Biomaterials Science and Engineering*. Plenum Press: NY.

Patin, D.J., Eckstein, E.C., Harum, K., and Pallares, V.S. (1993). Anatomic and biomechanical properties of human lumbar dura mater. Anesth. Analg. **76,** 535–540.

Petroll, W.M., Vishwanath, M., and Ma, L. (2004). Corneal fibroblasts respond rapidly to changes in local mechanical stress. Invest. Ophthalmol. Vis. Sci. **45,** 3466–3474.

Prange, M.T., and Margulies, S.S. (2002). Regional, directional, and age-dependent properties of the brain undergoing large deformation. J. Biomech. Eng. **124,** 244–252.

Runza, M., Pietrabissa, R., Mantero, S., Albani, A., Quaglini, V., and Contro, R. (1999). Lumbar dura mater biomechanics: experimental characterization and scanning electron microscopy observations. Anesth. Analg. **88,** 1317–1321.

Spicer, M.A., Van Velsen, M., Caffrey, J.P., and Apuzzo, M.L. (2004). Virtual reality neurosurgery: a simulator blueprint. Neurosurgery **54,** 783–797.

Stokes, B.T., and Jakeman, L.B. (2002). Experimental modelling of human spinal cord injury: a model that crosses the species barrier and mimics the spectrum of human cytopathology. Spinal Cord **40,** 101–109.

Stokes, B.T., Noyes, D.H., and Behrmann, D.L. (1992). An electromechanical spinal injury technique with dynamic sensitivity. J. Neurotrauma. **9,** 187–195.

Taylor, Z., and Miller, K. (2004). Reassessment of brain elasticity for analysis of biomechanisms of hydrocephalus. J. Biomech. **37,** 1263–1269.

Ueno, K., Melvin, J.W., Li, L., and Lighthall, J.W. (1995). Development of tissue level brain injury criteria by finite element analysis. J. Neurotrauma. **12,** 695–706.

Van Noort, R., Black, M.M., Martin, T.R., and Meanley, S. (1981). A study of the uniaxial mechanical properties of human dura mater preserved in glycerol. Biomaterials **2,** 41–45.

Vandenabeele, F., Creemers, J., and Lambrichts, I. (1996). Ultrastructure of the human spinal arachnoid mater and dura mater. J. Anat. **189,** 417–430.

Viidik, A. (1968). A rheological model for uncalcified parallel-fibred collagenous tissue. J. Biomech. **1,** 3–11.

Weed, L.H. (1938). Meninges and cerebrospinal fluid. J. Anat. **72,** 181–215.

Young, W. (2002). Spinal cord contusion models. Prog. Brain Res. **137,** 231–255.

Yuan, Q., Dougherty, L., and Margulies, S.S. (1998). *In vivo* human cervical spinal cord deformation and displacement in flexion. Spine **23,** 1677–1683.

Address reprint requests to:
David I. Shreiber, Ph.D.
Department of Biomedical Engineering
Rutgers, The State University of New Jersey
599 Taylor Road
Piscataway, NJ 08854

E-mail: shreiber@rci.rutgers.edu